Inorganic Chemistry

Article

pubs.acs.org/IC

Structural, Electronic, and Optical Properties of Eu-Doped BiOX (X = F, Cl, Br, I): A DFT+U Study

Zong-Yan Zhao* and Wen-Wu Dai

Faculty of Materials Science and Engineering, Key Laboratory of Advanced Materials of Yunnan Province, Kunming University of Science and Technology, Kunming 650093, People's Republic of China

ABSTRACT: In order to understand the photophysical properties and explain the experimental observations of Eu-doped BiOX (X = F, Cl, Br, I), the crystal structure, electronic structure, and optical properties of pure BiOX and Eu-doped BiOX have been calculated using the DFT+U method. By Eu doping, the band gap of BiOI is slightly narrowed, while the band gaps of others (BiOF, BiOCl, and BiOBr) are slightly broadened. Importantly, there is an isolated impurity energy band in the middle of the band gap, which is formed by seven spin-up energy levels of Eu-4f states. Furthermore, Eu doping enhances the internal electric fields of BiOX and makes the variation of band gaps and band widths become more outstanding, especially for the band widths of X-ns, O-2s, and Bi-6s related bands. Taking into account the energy level matching and band edge position, Eu-doped BiOCl is favorable not only for the photoluminescence application but also for the photocatalysis application. The findings in the present work could well explain the experimental observations in the literature and are helpful for the development of novel optoelectronic applications of BiOX-based materials.

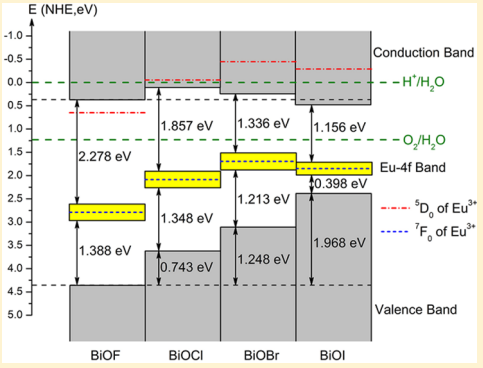

1. INTRODUCTION

In the past few decades, photocatalysis technology has attracted considerable attention in the fields of renewable energy development and environmental pollution treatment, leading to the development of efficient and practical photocatalysts becoming a rising hotspot. The current research works concentrate on the following aspects: (i) modifications for conventional photocatalysts (wide band gap semiconductors, such as TiO_2, ZnO, etc.), the main aim of which is to expand the photon response region to visible-light; the modification methods include ion doping, noble metal loading, heterojunction constructing, and dye sensitizing;[1,2] (ii) developments of novel photocatalysts, such as sulfides, oxysulfides, nitrides, oxynitrides, and oxyhalides, that have narrow band gaps, unique crystal structures, and excellent photoelectric properties.[3−5] For the latter strategy, Bi-based multiple compounds have drawn much attention for their potential applications for photocatalysis in recent years. Their typical representative is bismuth oxyhalides (BiOX, X = F, Cl, Br, I). BiOX has advantages of a unique crystal structure and excellent electronic and optical properties, and thus exhibits lots of important and promising applications, such as pigments in the cosmetic industry, magnetic materials, pharmaceuticals, phosphor, gas sensors, and catalysts in the oxidative coupling of methane reaction.[6−12]

BiOX is one of the simplest members of the Sillén family expressed by $[M_2O_2][X_m]$ that consists of analogous fluorite-like $[M_2O_2]$ layers that are intergrown with double halide $[X_m]$ layers.[13] Namely, its structure comprises a layer of $[Bi_2O_2]^{2+}$ slabs interleaved by double slabs of halogen ions $[X]^-$, forming [−X−Bi−O−O−Bi−X−] layers stacked one above the other by nonbonding van der Waals interaction through the halogen ions along the *c* axis.[14] This layered intergrowth structure can induce an internal static electric field between the $[Bi_2O_2]^{2+}$ slab and double $[X]^-$ slab along the *c* axis, which is believed to induce efficient separation of the photogenerated electron−hole pairs and thus is very advantageous for the photocatalytic activity of BiOX. In 2008, Zhang et al. prepared BiOX powders by employing a solvothermal process and evaluated their photocatalytic activities on the degradation of methyl orange.[8] They found that all the BiOX samples were photocatalytically active, and BiOI exhibited excellent activity under both UV-light and visible-light irradiation. In 2012, they synthesized a BiOCl single-crystalline nanosheet with exposed (001) and (010) facets by using a hydrothermal process and found that the sample with exposed (001) facets exhibited higher activity for direct semiconductor photoexcitation pollutant degradation under UV-light irradiation because of a cooperative effect between the surface atomic structure and suitable internal electric fields.[15] Since then, extensive interests have been focused on the syntheses and characterization of BiOX photocatalysts.[16,17]

In addition to photocatalytic performance, other optoelectronic applications of BiOX are equally compelling.[18] For example, the wide band gap of BiOCl could provide an optical window and the inherent quenching effects of rare earths, and importantly Bi could be a more favorable cation for rare earth ion dopant emission.[19−21] In 2008, Deng et al. first reported the strong blue photoluminescence centered at 455 nm with very high quantum yields (~0.4) from BiOCl nanomaterials at room

Received: September 3, 2014
Published: November 21, 2014

temperature.[22] Then, Cao et al. also found the principal green emission from the BiOCl film with a flowerlike hierachical structure, via 325 nm excitation.[23] And, Li et al. observed high multiphoto upconversion emission of Er^{3+} ions in Er-doped BiOCl or Er/Yb-codoped BiOCl microcrystals under 980 nm excitation.[24,25] During the past few decades, Eu^{3+} ion-doped phosphors were widely considered as an ideal substitute for the red component because of its good optical properties, such as its chemical stability and excellent color purity. When Eu^{3+} presents in a noncentrosymmetric site, materials containing Eu^{3+} have fluorescent emission peaks centered at about 610 nm, via a $^5D_0 \rightarrow {}^7F_2$ transition of the Eu^{3+} ion. Recently, Dash et al. studied the photoluminescence and photocatalytic activity of Eu^{3+}-doped BiOX (X = Cl, Br, I).[14] They observed that both Eu^{3+}-doped BiOCl and BiOBr nanoflakes exhibit strong optical properties (the asymmetric ratios of $^5D_0 \rightarrow {}^7F_2$ and $^5D_0 \rightarrow {}^7F_1$ transition) related to Eu^{3+} and Bi^{3+}, which are quenched in the case of the Eu^{3+}-doped BiOI matrix.

However, the mechanisms of photocatalysis and photoluminescence are opposite: photocatalytic reaction needs efficient separation of photogenerated electron−hole pairs, while photoluminescence occurs via the efficient recombination of photogenerated electron−hole pairs (i.e., radiative transition). This leads to an apparent puzzle: is Eu doping for BiOX beneficial to separation or recombination for the photogenerated electron−hole pairs? In other words, under what circumstance could Eu-doped BiOX be applied in the field of photocatalysis or photoluminescence? For example, Dash et al. have emphasized that the reason for the difference in optical characteristics of three Eu-doped BiOX's is unclear at this stage, and a more detailed study is needed to completely understand the experimental observations.[14] To the best of our knowledge, a few published articles are available to explore this open question. So, it is necessary to investigate and compare the relationship between electronic structure and photophysical properties of Eu-doped BiOX. Recently, some research groups have investigated the relationship between electronic structure and photocatalytic activity, using first-principles calculations.[26−28] On the other hand, other research groups attempted to investigate the photoluminescence properties of rare earth doped materials using first-principles calculations.[29−31] They obtained some successful results that are consistent with experimental observations, suggesting that theoretical calculations could be used to better understand the fundamental photophysical properties of Eu-doped BiOX. But the detailed doping effects of Eu-doped BiOX have still not been compared and provided. In our previous work, we preliminarily investigated the relationship between electronic structure and photoluminescence properties of Eu-doped BiOCl.[32] Motivated by the experimental work in ref 14, we believed that it is necessary to systematically study and compare the structural, electronic, and optical properties of Eu-doped BiOX, in order to develop efficient BiOX-based photocatalyst and photoelectric materials. Thus, in the present work, the crystal structure, electronic structure, and optical properties of Eu-doped BiOX were investigated by using density functional theory (DFT) calculations. Moreover, the relationship between electronic structure and photophysical properties will be discussed and compared. On the basis of the calculated results, possible explanations for previous experimental observations will be provided.

2. COMPUTATINAL METHODS

In the present work, a 3 × 3 × 2 supercell was constructed for the Eu-doped BiOX model, as shown in Figure 1. To build the

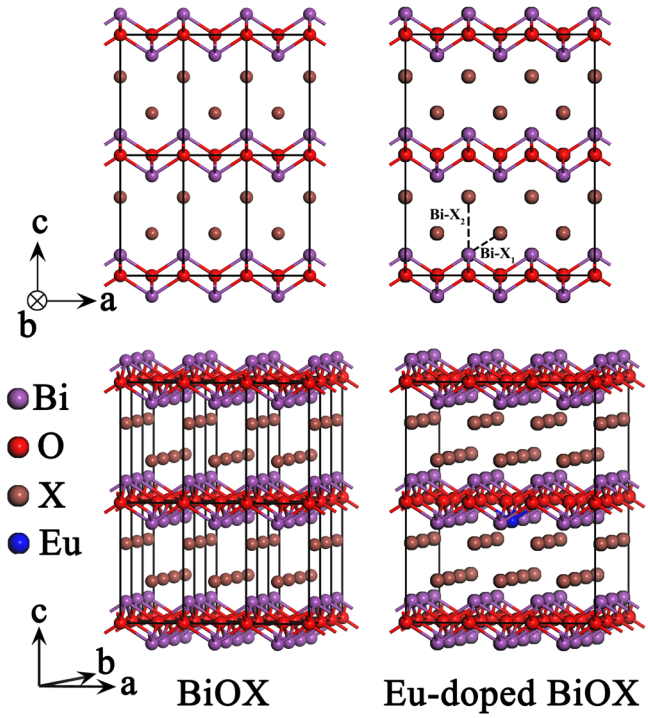

Figure 1. Crystal structure models of pure BiOX and Eu-doped BiOX (X = F, Cl, Br, I).

substitutional doping model, one Bi atom in the supercell was replaced by one Eu atom. Thus, every lattice parameter of the supercell model is larger than 10 Å, which could avoid the self-interaction of Eu impurity. In the supercell, the total number of atoms reached 108, and the corresponding Eu concentration is about 0.926% (atomic fraction). In fact, the Eu doping amount could achieve 5% in experiments.[14] Thus, this Eu doping amount could be comparable to that used in the experiments. To try to shield the atomic interaction between Eu impurities, and to highlight the mutual influence between Eu impurity and host atoms, the 3 × 3 × 2 supercell models were adopted in the present work.

In the present work, all of the calculations were carried out by using the periodic density functional theory package of Cambridge Serial Total Energy Package (CASTEP) codes.[33] CASTEP is a state-of-the-art quantum-mechanics-based program designed specifically for solid-state materials science. The core electrons (Bi and Eu, [Xe]; O and F, [He]; Cl, [Ne]; Br, [Ar]; I, [Kr]) were treated with the ultrasoft pseudopotential. The exchange-correlation effects of valence electrons (Bi, $6s^26p^3$; O, $2s^22p^4$; F, $2s^22p^5$; Cl, $3s^23p^5$; Br, $4s^24p^5$; I, $5s^25p^5$; and Eu, $4f^75s^25p^66s^2$) were described by the revised Perdew−Burke−Ernzerhof for solid (PBEsol) of generalized gradient approximation (GGA).[34] In order to obtain accurate electronic structure, the method of GGA+U was adopted to overcome the well-known shortcoming of GGA.[35] The Hubbard model is one of the most successful models to describe the correlated electrons in solids. To construct an appropriate functional, the GGA+U approach subdivides charge density into two subsystems: delocalized and localized. The former is described by its charge density, while for the latter a site diagonal charge

dx.doi.org/10.1021/ic5021059 | Inorg. Chem. 2014, 53, 13001−13011

Table 1. Lattice Distortion, Impurity Formation Energy, and Bond Length of Pure BiOX and Eu-doped BiOX (X = F, Cl, Br, I)[a]

					bond length/Å				average net charge/e				dipole moment/Debye	
	Δa /Å	Δc /Å	ΔV /Å^3	E_f /eV	Bi−O	Bi−X[b]	Eu−O	Eu−X[b]	Bi	O	X	Eu	BiO_4X_4	EuO_4X_4
pure BiOF					2.2769	2.7821, 2.7049			1.55	−0.89	−0.66		2.8089	
Eu-doped BiOF	−0.0012	−0.0125	−0.2297	−6.5212	2.2705	2.8021, 2.7060	2.3773	2.4842, 2.4370	1.54	−0.87	−0.64	0.99	2.9060	3.610
pure BiOCl					2.3111	3.0424, 3.5556			1.39	−0.90	−0.49		2.3336	
Eu-doped BiOCl	−0.0042	0.1332	1.7522	−4.6571	2.3045	3.0433, 3.7080	2.3470	2.9251, 3.5756	1.39	−0.89	−0.48	0.73	2.3045	2.6437
pure BiOBr					2.3180	3.1648, 4.3965			1.38	−0.89	−0.49		1.7033	
Eu-doped BiOBr	−0.0036	0.0354	0.2985	−3.9070	2.3126	3.1680, 4.4544	2.3037	3.0870, 4.4761	1.31	−0.87	−0.42	0.57	1.9950	2.1680
pure BiOI					2.3343	3.3515, 5.0948			1.19	−0.88	−0.31		2.4589	
Eu-doped BiOI	0.0116	0.0545	1.7341	−1.2594	2.3283	3.3609, 5.1735	2.3216	3.3418, 5.1807	1.19	−0.87	−0.29	0.35	2.4807	2.8748

[a]Their average net charge of every component by Mulliken's population analysis and the dipole moment of BiO_4X_4 or EuO_4X_4 polyhedra are also estimated. [b]The first value is the bond length of Bi or Eu with the first X layer atoms (as noted "Bi−X_1" in Figure 1); the second value is the bond length of Bi or Eu with the second X layer atoms (as noted "Bi−X_2" in Figure 1).

density matrix is introduced. In the present work, the value of U was set as follows: 4.8 eV for the p states of Bi and O, 15 eV for the p states of F, 7 eV for the p states of Cl, 3.5 eV for the p states of Br, 2.1 eV for the p states of I, and 4.8 eV for the f states of Eu, which is determined by comparison with available experimental measurements. The Monkhorst−Pack scheme K-points grid sampling was set as 4 × 4 × 2 for the irreducible Brillouin zone. A 60 × 60 × 80 mesh was used for fast Fourier transformation. An energy cutoff of 430 eV was used for expanding the Kohn−Sham wave functions. The Broyden−Fletcher−Goldfarb−Shanno (BFGS) scheme was chosen as the minimization algorithm.[36] Its convergence criteria were set as follows: the force on the atoms was less than 0.03 eV/Å; the stress on the atoms was less than 0.05 GPa; the atomic displacement was less than 1×10^{-3} Å, and the energy change per atom was less than 1×10^{-5} eV. On the basis of the optimized crystal structure, the electronic structure and the optical properties were then calculated. The band structures were calculated along the paths connecting the following high-symmetry points: Z(0,0,0.5) → A(0.5,0.5,0.5) → M(0.5,0.5,0) → Γ(0,0,0) → Z(0,0,0.5) → R(0,0.5,0.5) → X(0,0.5,0) → Γ(0,0,0) in the k-space. From the band structure to density of states, Gaussian broadening is applied to the eigenvalues, and the smearing width is set as 0.1 eV.

3. RESULTS AND DISCUSSION

3.1. Crystal Structure. The crystal structure of BiOX belongs to tetragonal matlockite PbFCl-type structure, with a symmetry of $P4/nmm$ (space group) or D_{4h}^7 (local symmetry). This is a layered intergrowth structure that is constructed by the combination of a double halogen ion layer and the bismuth oxygen layer, as shown in Figure 1. The Bi atom is coordinated to a square antiprism with four O atoms; the O atom is tetrahedrally coordinated to four Bi atoms, and the halogen atom is localized at the vertex of the pyramid that is formed with four Bi atoms in a planar square. However, the Bi−X bonds are very long (>3 Å) except in the case of BiOF, so there are no bonds between Bi atoms and halogen atoms in Figure 1. Its layered structure is exhibited by an ordered packing of the BiO_4 tetrahedron alternating with halogen atoms along the c axis direction, through the van der Waals interaction. Using the above-mentioned computational method, the lattice parameters of BiOX were obtained: $a = b = 3.7386$ Å and $c = 6.1714$ Å for BiOF, $a = b = 3.8743$ Å and $c = 7.3997$ Å for BiOCl, $a = b = 3.8996$ Å and $c = 8.4570$ Å for BiOBr, and $a = b = 3.9738$ Å and $c = 9.3722$ Å for BiOI, which are very consistent with experimental measurements,[7,14,37,38] suggesting that the computational method in the present work is reasonable.

For Eu-doped BiOX, the optimized parameters compared with pure BiOX are listed in Table 1. In the case of Eu-doped BiOF, both the a axis and c axis are slightly suppressed, so the cell volume is decreased, while in the case of Eu-doped BiOI, both the a axis and c axis are slightly expanded, so the cell volume is increased. And in the case of Eu-doped BiOCl or BiOBr, the a axis is slightly suppressed, while the c axis is slightly expanded, and the cell volume is increased. In general, for BiOX, the lattice distortions induced by Eu doping are not obvious, which is very important for BiOX to retain its unique structures and excellent optoelectric properties. For BiOF, the bond length between the Bi atom and F atom in the first layer (as noted "Bi−X_1" in Figure 1) is larger than the bond length between the Bi atom and F atom in the second layer (as noted "Bi−X_2" in Figure 1), owing to the smallest lattice parameter of c in BiOX. When the Eu impurity incorporates into the BiOX host lattice, all Bi−O bond lengths are shortened, while all Bi−X bond lengths are lengthened. Compared with Bi−O bond in pure BiOX or Eu-doped BiOX, all Eu−O bond lengths are longer than those of Bi−O bonds, while all bond lengths between Eu atoms and X atoms in the first layer are shorter than the bond lengths between Bi atoms and X atoms in the first layer. Due to the variation of the lattice parameter of the c axis, the bond length between the Eu atom and X atom in the second layer is shorter than the bond length between the Bi atom and the X atom in the second layer in Eu-doped BiOF and BiOCl, while the bond length between the Eu atom and X atom in the second layer is shorter than the bond length between the Bi atom and X atom in the second layer in Eu-doped BiOBr and BiOI.

In the DFT investigation, the conception of impurity formation energy (E_f) is usually used to determine the difficulty degree of impurity incorporated into the host crystal lattice,

dx.doi.org/10.1021/ic5021059 | Inorg. Chem. 2014, 53, 13001−13011

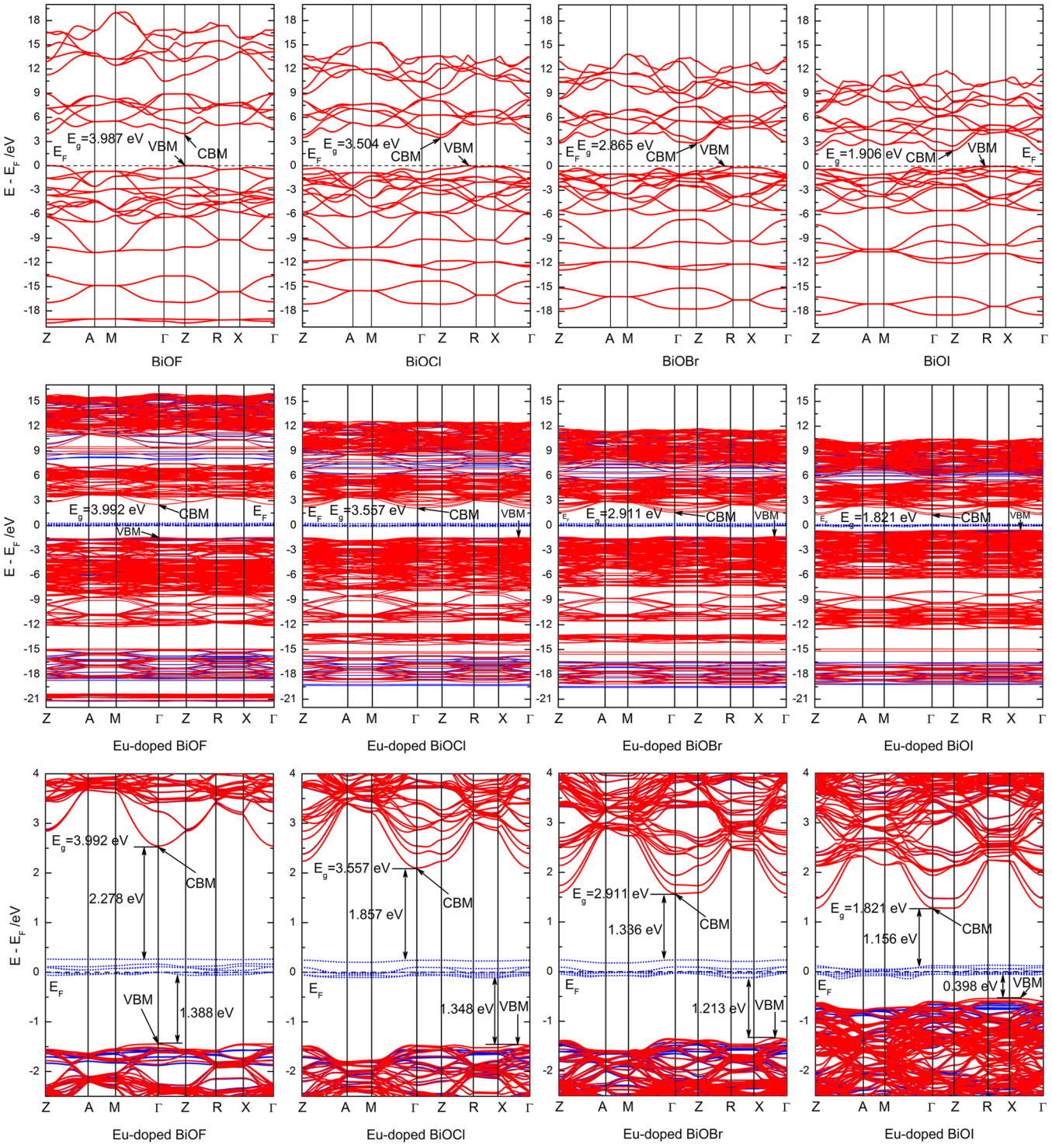

Figure 2. Calculated band structure of pure BiOX and Eu-doped BiOX (X = F, Cl, Br, I), and the corresponding distance between energy bands. The blue lines represent spin-up states, while the red lines represent spin-down states, in which the blue lines and red lines are completely coinciding in the case of pure BiOX.

which is a widely accepted approach. In the present work, the formula of impurity formation energy is referred to the formalism defined by Van de Walle et al.[39] And, the impurity formation energy of Eu-doped BiOX is also listed in Table 1. For all BiOX, the impurity formation energy of Eu is negative, implying that the process of Eu impurity incorporating into the host crystal lattice is an exothermic reaction. Thus, the preparation Eu-doped BiOX sample is not relatively problematic in experiments. Furthermore, the absolute value of E_f is decreasing with the increase in atomic number of halogen atoms.

The most important feature of BiOX is the open layered intergrowth crystal structure, which induces local internal fields through polarization of atoms in the space between these layers. This unique feature assists in effective separation of photogenerated electron−hole pairs, thus augmenting photocatalytic

dx.doi.org/10.1021/ic5021059 | Inorg. Chem. 2014, 53, 13001−13011

Table 2. Parameters of Band Structure of Pure BiOX and Eu-doped BiOX (X = F, Cl, Br, I)

		pure BiOF	Eu-doped BiOF	pure BiOCl	Eu-doped BiOCl	pure BiOBr	Eu-doped BiOBr	pure BiOI	Eu-doped BiOI
top of VB		Z	Γ	Z → R	X → Γ	Z → R	X → Γ	Z → R	X → Γ
bottom of CB		Z	Γ	Z	Γ	Z	Γ	Z	Γ
band gaps/eV	E_g (minimum)	3.9872	3.9919	3.5042	3.5567	2.8650	2.9112	1.9062	1.8208
	E_g (direct)	3.9872	3.9919	3.9106	3.5763	3.4753	2.9352	2.2825	1.8873
	O-2s → X-ns	2.0259[a]	1.7975[a]	1.3913	1.3226	2.2431	2.2101	4.1966	4.1302
	X-ns → Bi-6s	2.9059[b]	2.6547[b]	1.4393	1.3412	1.6767	1.5658	0.0064	−0.1216[c]
	Bi-6s → VB	−0.9006[c]	−0.2457[c]	−0.6419[c]	−0.4160[c]	0.5618	0.5401	1.3921	1.4862
	VB → Eu-4f		1.3876		1.3477		1.2135		0.3981
	Eu-4f → CB_L		2.2783		1.8572		1.3360		1.1561
	CB_L → CB_U	1.5634	1.8908	0.1638	0.4640	0.4598	0.9701	−0.0219[c]	0.0464
band width/eV	VB	7.1839	7.2019	6.4653	6.4768	6.0346	6.0665	5.8765	5.8897
	lower CB	4.9566	4.9231	4.6834	4.5896	4.5376	4.3430	4.3659	4.3503
	upper CB	8.5701	6.5716	6.9559	5.4499	6.0179	4.6848	5.5769	4.8487
	X-ns band	0.5037	0.8586	1.0329	1.1190	1.2689	1.3880	1.5097	2.0137
	O-2s band	3.2936	3.6430	2.8507	3.1655	2.5778	2.7377	2.2337	2.3317
	Bi-6s band	4.4822	3.8580	4.3892	3.6052	3.6279	3.5825	3.2192	2.7498
	Eu-4f band		0.3260		0.3518		0.3617		0.2741

[a]X-ns → O-2s. [b]O-2s → Bi-6s. [c]The negative value of the band gap indicates that the related bands are partially overlapping and represents the degree of overlapping.

efficiency of BiOX, because Sato et al. reported that the local internal fields due to the dipole moment of the distorted polyhedron can promote the charge separation in the very initial process of photoexcitation and are useful for enhancing photocatalytic activity.[40] With the Mulliken charges and lattice parameters, the absolute values of the dipole moments for the BiO_4X_4 polyhedra within relaxed pure BiOX are estimated and listed in Table 1. In the present work, we found that BiOF has the largest dipole moment (2.81 D), while BiOBr has the smallest dipole moment (1.70 D). These data are consistent with previous reports.[41,42] Furthermore, when Eu impurity incorporates into the BiOX host lattice, the electrons will be redistributed, in addition to the lattice distortion induced by the differences of ion radius and valence electron. In Table 1, the average net charge on different component atoms is displayed. First, the average net charge on the atoms in Eu-doped BiOX is slightly decreasing, compared with the corresponding pure BiOX. Second, the average net charge on Eu impurity is obviously smaller than that of the Bi atom. And this value is decreasing along with increasing of the atomic number of the halogen. In particular, the variation of average net charge of atoms is a local effect. In other words, compared with pure BiOX, the variation of average net charge of atoms that neighbor Eu impurity is more obvious, while the variation average net charge of atoms that are far away from Eu impurity is not obvious, almost even equalling that of pure BiOX. Therefore, the local internal fields of BiO_4X_4 and EuO_4X_4 polyhedra of Eu-doped BiOX are larger than that of pure BiOX, as shown in Table 1. And the orders of dipole moment of BiO_4X_4 and EuO_4X_4 polyhedra of Eu-doped BiOX are identified with that of pure BiOX.

3.2. Electronic Structure. The band structures of pure BiOX and Eu-doped BiOX are illustrated in Figure 2. The energy zero (i.e., the Fermi energy level, E_F) is set at the valence band maximum (VBM). In the case of pure BiOF, both the VBM and conduction band minimum (CBM) are located at the k-point of Z, indicating that pure BiOF is a direct band gap semiconductor. While, in the case of pure BiOCl, BiOBr, and BiOI, the VBM is located on the k-point line of Z → R, and the CBM is located at the k-point of Z, indicating they are indirect band gap semiconductors. At the same time, the spin-up states and the spin-down states are completely coincident, owing to the pairing electrons in pure BiOX, while the spin up states and the spin down states are not coincident in the cases of Eu-doped BiOX. The calculated minimum band gap (E_g), the distance between VBM and CBM, is 3.987 eV for BiOF, 3.504 eV for BiOCl, 2.865 eV for BiOBr, and 1.906 eV for BiOI (if using standard DFT calculations, the band gaps of BiOX are respectively obtained as follows: 3.072 eV for BiOF, 2.521 eV for BiOCl, 2.182 eV for BiOBr, and 1.591 eV for BiOI), which are very consistent with experimental measurements (~3.46−3.51 eV of BiOCl, ~2.9 eV for BiOBr, and ~1.9 eV for BiOI).[27,43−46] Namely, the band gap of BiOX is decreasing along with the increase of X atomic number. In the published literature, some research groups have calculated the electronic structures of pure BiOX via standard DFT calculations, and obtained the underestimated band gaps: 2.79−3.34 eV for BiOF, 2.34−2.92 eV for BiOCl, 1.99−2.65 eV for BiOBr, and 1.38−1.75 eV for BiOI. The VB top and CB bottom are almost independent of the involvement of Bi 5d and Bi 5f states.[26−28,41,47−49] Compared with these calculated results, the band gaps of BiOX could be accurately reproduced in the present work via DFT+U method.

By Eu doping, the values of E_g are slightly increased, except Eu-doped BiOI. And the types of band gaps are not changed, besides the position shifting of VBM and CBM in BiOCl, BiOBr, BiOI, as shown in Figure 2 and Table 2. In the present work, the direct band gaps of BiOX are also evaluated as listed in Table 2. In the cases of pure BiOX, the difference between minimum E_g and direct E_g is obvious (>0.35 eV), while this difference is small (~0.03 eV) in the cases of Eu-doped BiOX. For the photoelectronic applications of BiOX, the value and type of band gap are important: the value of the band gap determines the response range for solar light; a direct band gap is favorable for the absorption of photon energy, while an indirect band gap is favorable for the separation of photo-generated electron−hole pairs. In the cases of Eu-doped BiOX, there is an impurity energy band in the middle of the band gap,

dx.doi.org/10.1021/ic5021059 | Inorg. Chem. 2014, 53, 13001−13011

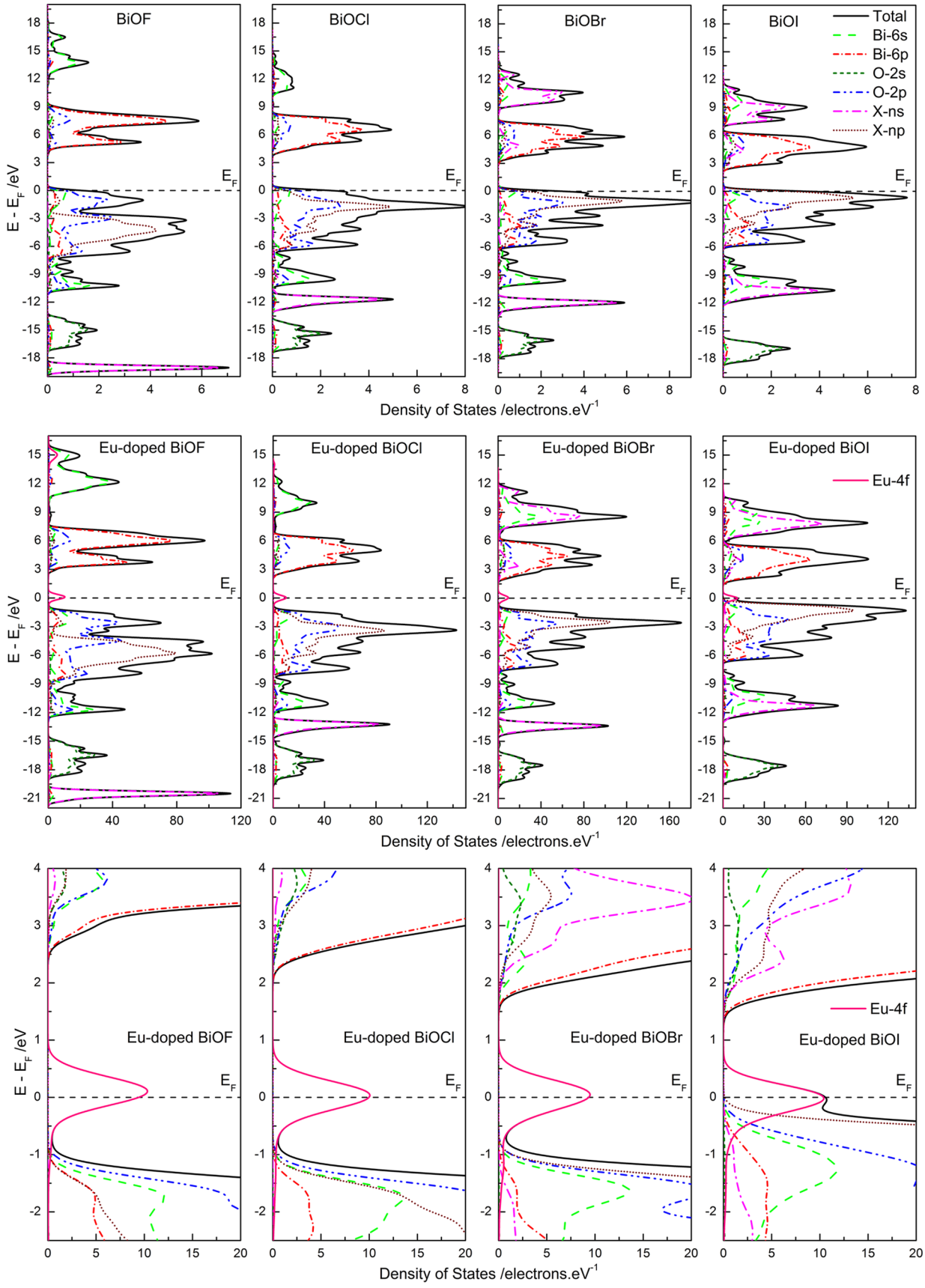

Figure 3. Calculated total and partial density of states of pure BiOX and Eu-doped BiOX (X = F, Cl, Br, I).

which is formed by seven spin-up energy levels. The Fermi energy level crosses these impurity energy bands, indicating that they are half occupied energy bands. This phenomenon is attributed to the Eu-4f states being only partially filled; even in

dx.doi.org/10.1021/ic5021059 | Inorg. Chem. 2014, 53, 13001−13011

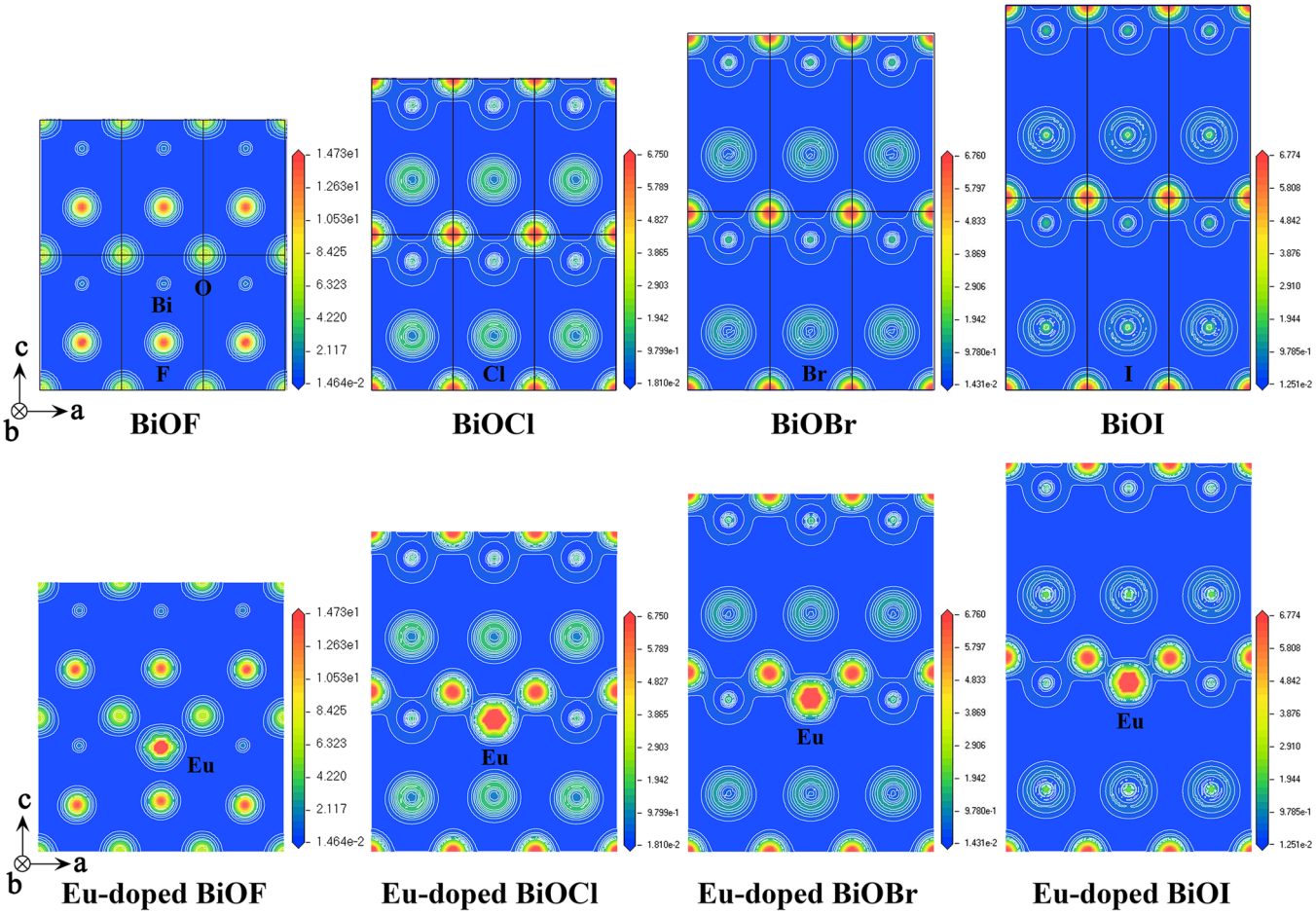

Figure 4. Electron density maps of pure BiOX and Eu-doped BiOX (X = F, Cl, Br, I).

the Eu-doped BiOX system, Eu loses some electrons, as shown in Table 1. However, the possibility of photogenerated carriers on this impurity energy band is very small, due to its very weak peak of density of states (DOS) compared with that of the host. Therefore, it could not obviously influence the light-absorption properties and the transfer behavior of photogenerated carriers in the BiOX host. The distances between the bottom (or top) of this impurity energy band and VBM (or CBM) are estimated and listed in Table 2. According to these data, except Eu-doped BiOI, the impurity energy band belongs to the deep energy band, implying that it may act as a recombination center for the photogenerated electron−hole pair in heavy Eu doping due to the equivalent transition probability of electrons from CB to it and holes from VB to it. In particular, the impurity energy band acts as the acceptor in the case of Eu-doped BiOI, because the distance from VBM to it is only ∼0.4 eV and partially overlapping with VB (as discussed below). Thus, the impurity energy band in Eu-doped BiOI is favorable for the photon absorption and the separation of photogenerated electron−hole pairs. These calculated results imply that Eu incorporating into the BiOX host induces the impurity energy band as well as retains the main features of electronic structure of BiOX. Thus, in Figures 2 and 3, we used a wide energy range for pure BiOX and Eu-doped BiOX to exhibit the basic features of electronic structure (including energy bands in different energy ranges, the composition and shifting of different energy bands, chemical bonding information, and so on). At the same time, we used a narrow energy range for Eu-doped BiOX to highlight the changes of electronic structure around the band gap, especially the position and composition of the Eu-related impurity energy band.

Combined with the above-mentioned band structures, the total and partial DOS of pure BiOX and Eu-doped BiOX are plotted in Figure 3, in order to analyze the chemical bonding information. For pure BiOF, in the range of −19.5 to −19 eV, the DOS peak is predominately contributed by F-2s states. As X atomic number increasing, the X-ns related DOS peak (or X-ns band) is up-shifting. In the case of BiOF, the F-2s related band is below the O-2s related band, while in the cases of BiOCl, BiOBr, and BiOI, the X-ns related band is above the O-2s related band. Finally, the I-5s related band is partially overlapping with the Bi-6s related band, as shown in Figure 3. So along with the increase of X atomic number, the distance between the X-ns related band and the Bi-6s related band (noted as "X-ns → Bi-6s band gap" in Table 2) is decreased, and the bandwidth of the X-ns related band is broadening. Furthermore, Eu-doping makes these effects more obvious. In other words, the distance between the X-ns related band and Bi-6s related band in Eu-doped BiOX is smaller than that in pure BiOX, and the bandwidth of the X-ns related band in Eu-doped BiOX is wider than that in pure BiOX, as listed in Table 2. The O-2s and Bi-6s related bands are respectively located at −18 to −14 eV and −10 to −7 eV, and the band widths are narrowing along with the increase of X atomic number (in the cases of Eu-doped BiOX, this effect is more obvious). Owing to the X-ns related band up-shifting, the distance between the O-

dx.doi.org/10.1021/ic5021059 | Inorg. Chem. 2014, 53, 13001−13011

2s related band and X-ns related band is increasing, while the distance between the Bi-6s related band and X-ns related band is decreasing, along with the increase of X atomic number. The O-2p states, X-np states, and Bi6p states contribute considerably to the formaiton of VB, in which the contribution of O-2p states is predominant. In other words, the hybridization states between Bi6p states and O-2p states or X-np states dominantly compose the middle part of VB. Meanwhile, at the bottom of VB, Bi6p states also exhibit hybridization with O-2p states or X-np states. The top of VB predominately consists of the hybridization states between O-2p states or X-np states and Bi-6s states. And as the X atomic number increases, the X-np states are up-shifting and finally contribute for the formation of the top of VB; in other words, X-np states do not contribute to the formation of the top of VB in the cases of BiOF and BiOCl, while they contribute for the formation of the top of VB in the cases of BiOBr and BiOI. The CB of BiOX is divided into two parts: the lower part of CB (CB_L) is mainly composed by the Bi6p states; in particular, the bottom of CB is the antibonding states of Bi6p states. The upper part of CB (CB_U) is mainly composed of Bi-6s states in the cases of BiOF and BiOCl, while it is mainly composed of X-ns states in the cases of BiOBr and BiOI. For pure BiOX, the bandwidth of VB and CB is decreasing, and the band gap between VB and CB_L (or CB_L and CB_U) is narrowing, along with the increase of X atomic number. Eu-doping significantly changes the band gaps but does not obviously alter the bandwidth of VB or CB. These bonding features are in accord with previously published results that obtained by different research groups.[26−28,41,47−49] For example, Huang et al. carried out a series of calculating works and found that the CB bottom flattens with the increase in X atomic number of BiOX. Furthermore, they concluded that both O-2p and X-np states dominated the VB, while Bi6p states contribute most to the CB. And the localized X-np states in the VB shift toward the VB top with the increase of X atomic number, along with certain changes in the VB and CB bandwidths. The calculated results of pure BiOX in the present work are very well consistent with these published results in the literature, suggesting that the calculated results of Eu-doped BiOX will be reliable and reasonable.

In the cases of Eu-doped BiOX, the main bonding features are still exhibited and maintained. It is worth notice that the impurity energy band is absolutely overall composed by the Eu-4f states, as shown in Figure 3. Combined with the calculated band structure, this impurity energy band could be considered isolated and localized states (the corresponding bandwidth is ~0.3 eV). Another difference compared with that of pure BiOX is that the Fermi energy level is relatively upward shifting, because more valence electrons are induced by the Eu impurity.

To further explore the properties of electronic structure, the electron density maps of pure BiOX and Eu-doped BiOX are also plotted in Figure 4. Except in the case of BiOF, the electron density between O atoms and Bi atoms is slightly larger than that of the background, indicating there are mixed bonds (mainly ionic bond plus a certain of covalent bond) between O atoms and Bi atoms. The electron density between X atoms and Bi atoms is equivalent to that of the background, indicating there are complete ionic bonds between X atoms and Bi atoms, as well as O atoms and Bi atoms in the case of BiOF. The electron density around O atoms is much larger than that of around Bi atoms or X atoms, meaning that more electrons aggregate around O atoms. Thus, the direction of electron transfer is from Bi atom to O atom. Meanwhile, the gain of electrons around X atoms is very low. In order to quantitatively express these characteristics, the average net charge on atoms by Mulliken's population analysis is also listed in Table 1. As X atomic number increases, the features of the covalent band are more and more obvious, as shown in Figure 4 and Table 1. When the Eu impurity incorporates into the BiOX host lattice, it is obviously observed that the electron density around the Eu impurity is extended farther than around Bi atoms. The electron density around O atoms and X atoms is not obviously changed, compared with the situation in pure BiOX. The principal variation induced by Eu impurity incorporation is the weakening of the covalent bond feature between O atoms and Bi atoms near the Eu impurity. However, the bonding features of Bi−O bonds, which are far away from the Eu impurity, are still maintained. At the same time, the features of the covalent bond between O atoms and the Eu atom are much stronger than that between O atoms and Bi atoms in pure BiOX and Eu-doped BiOX. These results are also included in Figure 4 and Table 1. Taking into account these calculated results, one can draw a conclusion that the doping effects of the Eu impurity are very localized for BiOX.

3.3. Photophysical Properties. The calculated absorption spectra of pure BiOX and Eu-doped BiOX by the polycrystalline models as displayed in Figure 5, which are consistent with

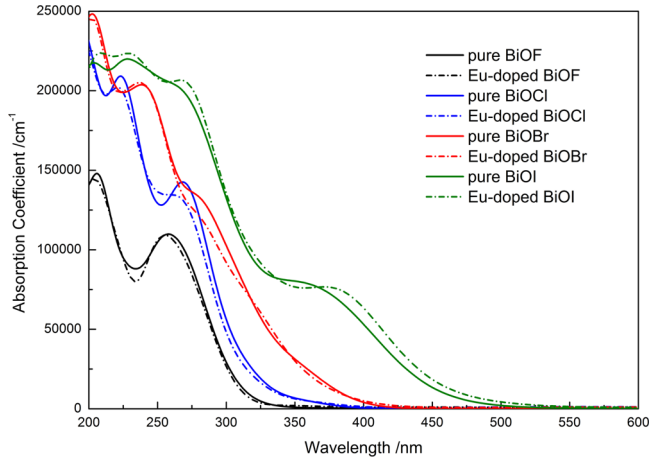

Figure 5. Calculated absorption spectrum of pure BiOX and Eu-doped BiOX (X= F, Cl, Br, I).

reported experimental observations.[8,14,43] As above-mentioned about band structures, the band gaps of Eu-doped BiOX (X = F, Cl, Br) are slightly broadened, compared with pure BiOX. Thus, the fundamental absorption energy edge of Eu-doped BiOX (X = F, Cl, Br) is slightly blue-shifting. To the contrary, the band gap of Eu-doped BiOI is narrowed, resulting in the red-shifting of the fundamental absorption energy edge, compared with those of pure BiOI. Because the shifting of fundamental absorption energy edges is not obvious in the cases of Eu-doped BiOX, these calculated results mean that Eu impurity incorporated into the BiOX host lattice does not charge the broadband absorption property of BiOX, which can absorb the entirety of incident light whose photon energy is greater than the band gap. These calculated results are in very good agreement with previous experimental measurements.[14] Therefore, introducing the luminescence center does not influence the excitation properties of the host for the luminescence application of BiOX, and more incident photon energy could be converted to light-emitting Eu^{3+} via the charge

dx.doi.org/10.1021/ic5021059 | Inorg. Chem. 2014, 53, 13001−13011

transfer and energy transfer, if there is appropriate energy level matching, as discussed below.

As shown in Figure 1, the [−X−Bi−O−O−Bi−X−] layers are stacked together by the nonbinding interaction through the X atoms along the *c* axis. Therefore, the structure is not closely packed in this direction. When one photon excites one electron from the hybridized states of Bi-6s with X-np states or O-2p states to Bi6p states on the top of VB, one pair of a hole and an excited electron appear. The intrinsic internal electric fields between positive $[Bi_2O_2]^{2+}$ and double negative X^- layers could provide a large enough space to polarize the related atoms and orbitals and, consequently, improve the separation efficiency of photogenerated electron−hole pairs. The loosely packed structure, indirect band gap, and intrinsic internal electric field benefit the photogenerated electron−hole pair's separation and the charge transition. This is the reason why BiOX could be an excellent photocatalyst. As for the application of photoluminescence, these features also could play a principal role. Owing to the efficient separated photogenerated electron−hole pairs, the probability of charge transfer from host to luminescence center may increase. Namely, if the energy levels of the luminescence center could be matched with the energy bands, the energy transport and charge transfer could efficiently take place.

Combined with above discussions, the energy levels diagram of Eu-doped BiOX is proposed in Figure 6. In the present work,

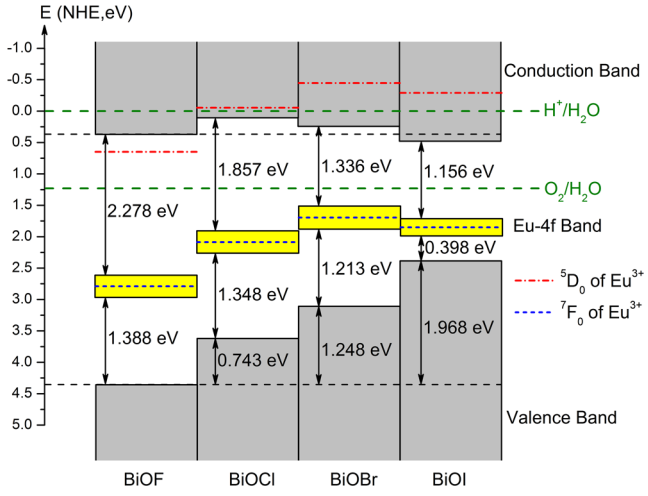

Figure 6. Proposed energy level diagram of pure BiOX and Eu-doped BiOX (X = F, Cl, Br, I).

the band offset or band alignment is estimated by the procedure proposed in refs 50 and 51. As shown in Figure 6, the band edge positions of BiOF are set as references. The outstanding feature of BiOX is that the shifting of the bottom of CB is not obvious, while the top of VB is considerably up-shifted along with the increase of the X atomic number. The reason is just the composition of the band structure: the bottom of CB consists of the Bi6p antibonding states in all BiOX, which is relatively fixed; while the top of VB consists of the hybridization states between O-2p states or X-np states and Bi-6s states, and the X-np states will be up-shifting along with the increase of X atomic number. The Eu-4f related impurity energy band and the position of energy levels ($^7F_0$ as the ground state and $^5D_0$ as the lowest excited state) of Eu^{3+} are plotted in Figure 6. In the case of BiOF and BiOCl, the position of $^5D_0$ of Eu^{3+} is just below or above the bottom of CB (the distances are less than 0.28 eV), implying that the energy levels of the luminescence center (Eu^{3+}) are matched with the energy bands of the host (BiOF or BiOCl). As previously published reports, the spectrum of BiOCl displays an emission peak in the range of 340−420 nm, under a 320 nm excitation,[10] which is overlapping with the charge transfer states of Eu^{3+}. Therefore, these effects guarantee that the photogenerated electrons on the bottom of CB could be transferred to the lowest excited state ($^5D_0$) of Eu^{3+}. At the same time, the incident energy is also transported from host to luminescence center. On the contrary, in the cases of BiOBr and BiOI, the $^5D_0$ position of Eu^{3+} is above the bottom of CB by a center distance (larger than 0.70 eV), implying that the energy levels of the luminescence center (Eu^{3+}) are mismatched with the energy bands of the host (BiOBr or BiOI). Thus, the photogenerated electrons on the bottom of CB cannot efficiently transfer to the lowest excited state of Eu^{3+}. For the photocatalysis application, the Eu-4f related impurity energy band is just above the top of VB, and partially overlapping with it, which is favorable for the transfer of photogenerated carriers to reactive sites at the catalyst surface with their lifetime,[2] but the ability of a semiconductor to undergo photogenerated electron transfer to adsorbed species on its surface is governed by the band energy position of the semiconductor and the redox potentials of the adsorbate. The relevant potential level of the acceptor is thermodynamically required to be below (more positive than) the conduction band potential of the semiconductor. The potential level of the donor needs to be above (more negative than) the valence band position of the semiconductor in order to donate an electron to the vacant hole.[52] According to this principle, one could find that the pure BiOCl and Eu-doped BiOCl is favorable for the photocatalysis application, because their CBM (at 0.107 and 0.067 eV) is just below the H^+/H_2O level. Other BiOX CBMs are located at 0.367 eV for BiOF, 0.242 eV for BiOBr, and 0.487 eV for BiOI. By Eu doping, their CBM is slightly up-shifting, except Eu-doped BiOI (0.350 eV for Eu-doped BiOF, 0.067 eV for Eu-doped BiOCl, 0.206 eV for Eu-doped BiOBr, and 0.516 eV for Eu-doped BiOI). These calculated results could well explain the underlying mechanism of experimental observations by Dash et al.:[14] Eu-doped BiOCl exhibits strong optical properties, which are quenched in the case of Eu-doped BiOI, and the Eu-doped BiOCl manifested higher photocatalystic efficiency compared to Eu-doped BiOBr and BiOI.

Going back to the open question mentioned in the Introduction, the reasons that the doping effects of Eu in BiOCl are favorable for photocatalysis as well as photoluminescence are based on the following aspects: (1) The enhanced built-in electric field can improve the separation of photogenerated electron−hole pairs, resulting in inhibition of the intrinsic recombination. In the case of photocatalysis, this effect is undoubtedly advantageous. And in the case of photoluminescence, the decreased intrinsic recombination means there are more photogenerated electrons or holes that could transfer to the luminescence center of the Eu impurity, resulting in enhancement of the emission intensity. (2) For photocatalysis, the key requirement of the redox reaction is the band edge position. Compared with the pure BiOX system, the position of the conduction band of the Eu-doped BiOX system is relatively upward shifting, suggesting that its reducing activity will be enhanced. For photoluminescence, the key factor is efficient energy transport and charge transfer. In the case of Eu-doped BiOCl, the distance between the bottom of the

dx.doi.org/10.1021/ic5021059 | *Inorg. Chem.* 2014, 53, 13001−13011

conduction band of BiOCl and the lowest excited energy level of $^5D_0$ is very small (namely, the existence of energy level matching between them), which ensures that the energy transport and charge transfer could be effectively carried out. (3) As discussed above, the doping effect of Eu in the BiOX host is an obvious local effect; in particular, the photoluminescence phenomenon only occurs at the luminescence center (Eu impurity). Therefore, when the photogenerated carriers reach the surface and transfer to adsorbates, the photocatalysis will take place; when the photogenerated carriers meet the luminescence center, the photoluminescence will take place. In other words, the photocatlysis is mainly related with the host materials of BiOX, in which the Eu impurity adjusts the crystal structure, electronic structure, and optical properties, while the emission properties of photoluminescence are mainly related with the luminescence center (Eu impurity), in which the host materials of BiOX absorb the incident photon energy and transfer the photogenerated carriers and energy to the luminescence center. Recently, a similar phenomenon is observed in the case of Tb^{3+}-doped TiO_2,[53] indicating that photocatalysis and photoluminescence could be enhanced in the same system, although their mechanisms are different from each other. On the basis of the relationship between materials properties and photocatalysis or photoluminescence, Eu doping could obviously improve the photocatalytic activity of BiOCl, as well as exhibit a strong emission intensity of photoluminescence.

4. SUMMARY AND CONCLUSIONS

In order to understand the photophysical properties and mechanism of Eu-doped BiOX (X = F, Cl, Br, I), the crystal structure, electronic structure, and optical properties of pure BiOX and Eu-doped BiOX have been calculated using the DFT +U method. The lattice distortions of BiOX are not obvious with Eu impurity incorporation. And, the process of Eu impurity incorporation into the host crystal lattice is an exothermic reaction. Thus, the preparation of Eu-doped BiOX samples is relatively unproblematic in experiments. By Eu doping, the band gap of BiOI is slightly narrowed, while the band gaps of others (BiOF, BiOCl, and BiOBr) are slightly broadened. Importantly, there is an isolated impurity energy band in the middle of the band gap, which is formed by seven spin-up energy levels of Eu-4f states. Owing to the unique layered structure, the BiOX host could produce enough separated electron−hole pairs by the internal electric fields, which are enhanced by Eu doping. As the X atomic number increases, the X-ns or -np related bands are up-shifting and contribute the composition of the upper conduction band or the top of the valence band, resulting in the fundamental band gap narrowing or BiOX. Most other band gaps between different electronic states related bands are also narrowing; the band widths of the O-2s related band, Bi-6s related band, valence band, and conduction band are narrowing, while those of the X-ns related band and Eu-4f related band are broadening. Importantly, Eu doping makes these effects become more outstanding, especially for the band widths of X-ns, O-2s, and Bi-6s related bands. Taking into account the energy level matching, it can be found that the lowest excited state ($^5D_0$) of Eu^{3+} is very close to the bottom of the conduction band of BiOCl, so the energy transport and charge transfer could be efficiently carried out, resulting in the photogenerated electrons at the multiplets of Eu^{3+} being able to produce strong orange-red emissions via radiative relaxation. On the other hand, the Eu doping makes BiOCl have stronger reducing activity, owing to the bottom of the conduction band of Eu-doped BiOCl being more negative. The findings in the present work could well explain the experimental observations in the literature and are helpful for the development of novel optoelectronic applications of BiOX-based materials.

AUTHOR INFORMATION

Corresponding Author

*Tel.: +86-871-65919924. Fax: +86-871-65107922. E-mail: zzy@kmust.edu.cn.

Notes

The authors declare no competing financial interest.

ACKNOWLEDGMENTS

The authors would like to acknowledge financial support from the National Natural Science Foundation of China (Grant No. 21263006, 21473082).

REFERENCES

(1) Chen, X.; Mao, S. S. *Chem. Rev.* **2007**, *107*, 2891−2959.
(2) Asahi, R.; Morikawa, T.; Ohwaki, T.; Aoki, K.; Taga, Y. *Science* **2001**, *293*, 269−271.
(3) Zhao, Z.; Li, Z.; Zou, Z. *Phys. Chem. Chem. Phys.* **2011**, *13*, 4746−4753.
(4) Zou, Z.; Ye, J.; Sayama, K.; Arakawa, H. *Nature* **2001**, *414*, 625−627.
(5) Li, G.; Bai, Y.; Zhang, W. F.; Zhang, H. *Mater. Chem. Phys.* **2013**, *139*, 1009−1013.
(6) Briand, G. G.; Burford, N. *Chem. Rev.* **1999**, *99*, 2601−2658.
(7) Kijima, N.; Matano, K.; Saito, M.; Oikawa, T.; Konishi, T.; Yasuda, H.; Sato, T.; Yoshimura, Y. *Appl. Catal., A* **2001**, *206*, 237−244.
(8) Zhang, X.; Ai, Z.; Jia, F.; Zhang, L. *J. Phys. Chem. C* **2008**, *112*, 747−753.
(9) Deng, Z.; Chen, D.; Peng, B.; Tang, F. *Cryst. Growth Des.* **2008**, *8*, 2995−3003.
(10) Zhang, K.; Liang, J.; Wang, S.; Liu, J.; Ren, K.; Zheng, X.; Luo, H.; Peng, Y.; Zou, X.; Bo, X.; Li, J.; Yu, X. *Cryst. Growth Des.* **2011**, *12*, 793−803.
(11) Chen, L.; Huang, R.; Xiong, M.; Yuan, Q.; He, J.; Jia, J.; Yao, M.-Y.; Luo, S.-L.; Au, C.-T.; Yin, S.-F. *Inorg. Chem.* **2013**, *52*, 11118−11125.
(12) Michel, C. R.; López Contreras, N. L.; Martínez-Preciado, A. H. *Sens. Actuators, B* **2012**, *173*, 100−105.
(13) Kusainova, A. M.; Zhou, W.; Irvine, J. T. S.; Lightfoot, P. *J. Solid State Chem.* **2002**, *166*, 148−157.
(14) Dash, A.; Sarkar, S.; Adusumalli, V. N. K. B.; Mahalingam, V. *Langmuir* **2014**, *30*, 1401−1409.
(15) Jiang, J.; Zhao, K.; Xiao, X.; Zhang, L. *J. Am. Chem. Soc.* **2012**, *134*, 4473−4476.
(16) Cheng, H.; Huang, B.; Dai, Y. *Nanoscale* **2014**, *6*, 2009−2026.
(17) Ye, L.; Su, Y.; Jin, X.; Xie, H.; Zhang, C. *Environ. Sci. Nano* **2014**, *1*, 90−112.
(18) Auzel, F. *Chem. Rev.* **2003**, *104*, 139−174.
(19) Patra, A.; Friend, C. S.; Kapoor, R.; Prasad, P. N. *J. Phys. Chem. B* **2002**, *106*, 1909−1912.
(20) Zhang, L.; Wang, W.; Sun, S.; Zhang, Z.; Xu, J.; Ren, J. *Catal. Commun.* **2012**, *26*, 88−92.
(21) Cao, Y.; Zhao, Z.; Yi, J.; Ma, C.; Zhou, D.; Wang, R.; Li, C.; Qiu, J. *J. Alloys Compd.* **2013**, *554*, 12−20.
(22) Deng, Z.; Tang, F.; Muscat, A. *Nanotechnology* **2008**, *19*, 295705.
(23) Cao, S.; Guo, C.; Lv, Y.; Guo, Y.; Liu, Q. *Nanotechnology* **2009**, *20*, 275702.
(24) Li, Y.; Song, Z.; Li, C.; Wan, R.; Qiu, J.; Yang, Z.; Yin, Z.; Yang, Y.; Zhou, D.; Wang, Q. *Appl. Phys. Lett.* **2013**, *103*, 231104.

(25) Li, Y.; Song, Z.; Li, C.; Wan, R.; Qiu, J.; Yang, Z.; Yin, Z.; Yang, Y.; Wang, X.; Wang, Q. *Ceram. Int.* **2013**, *39*, 8911−8916.
(26) Huang, W. L.; Zhu, Q. *Comput. Mater. Sci.* **2008**, *43*, 1101−1108.
(27) Zhang, K.-L.; Liu, C.-M.; Huang, F.-Q.; Zheng, C.; Wang, W.-D. *Appl. Catal., B* **2006**, *68*, 125−129.
(28) Zhao, L.; Zhang, X.; Fan, C.; Liang, Z.; Han, P. *Phys. B: Condens. Matter* **2012**, *407*, 3364−3370.
(29) Mikami, M.; Oshiyama, A. *J. Lumin.* **2000**, *87*−*89*, 1206−1209.
(30) Toyoshima, H.; Watanabe, S.; Ogasawara, K.; Yoshida, H. *J. Lumin.* **2007**, *122*−*123*, 104−106.
(31) Zhang, J.; Zhou, M.; Qin, Q.; Yu, M.; Wang, Y. *J. Lumin.* **2011**, *131*, 1636−1640.
(32) Yi, J.; Zhao, Z.-Y. *J. Lumin.* **2014**, *156*, 205−211.
(33) Clark, S. J.; Segall, M. D.; Pickard, C. J.; Hasnip, P. J.; Probert, M. J.; Refson, K.; Payne, M. C. *Z. Kristallogr.* **2005**, *220*, 567−570.
(34) Perdew, J. P.; Ruzsinszky, A.; Csonka, G. I.; Vydrov, O. A.; Scuseria, G. E.; Constantin, L. A.; Zhou, X.; Burke, K. *Phys. Rev. Lett.* **2008**, *100*, 136406.
(35) Anisimov, V. I.; Zaanen, J.; Andersen, O. K. *Phys. Rev. B* **1991**, *44*, 943.
(36) Pfrommer, B. G.; Côté, M.; Louie, S. G.; Cohen, M. L. *J. Comput. Phys.* **1997**, *131*, 233−240.
(37) Keramidas, K.; Voutsas, G.; Rentzeperis, P. *Z. Kristallogr.* **1993**, *205*, 35−40.
(38) Keller, E.; Krämer, V. *Z. Naturforsch. B* **2005**, *60b*, 1255.
(39) Van de Walle, C. G.; Neugebauer, J. *J. Appl. Phys.* **2004**, *95*, 3851−3879.
(40) Sato, J.; Kobayashi, H.; Inoue, Y. *J. Phys. Chem. B* **2003**, *107*, 7970−7975.
(41) Huang, W. L. *J. Comput. Chem.* **2009**, *30*, 1882−1891.
(42) Zhang, H.; Liu, L.; Zhou, Z. *Phys. Chem. Chem. Phys.* **2012**, *14*, 1286−1292.
(43) Wang, W.; Huang, F.; Lin, X. *Scripta Mater.* **2007**, *56*, 669−672.
(44) Wang, W.; Huang, F.; Lin, X.; Yang, J. *Catal. Commun.* **2008**, *9*, 8−12.
(45) Henle, J.; Simon, P.; Frenzel, A.; Scholz, S.; Kaskel, S. *Chem. Mater.* **2007**, *19*, 366−373.
(46) Lin, X.; Shan, Z.; Li, K.; Wang, W.; Yang, J.; Huang, F. *Solid State Sci.* **2007**, *9*, 944−949.
(47) Huang, W. L.; Zhu, Q. *J. Comput. Chem.* **2009**, *30*, 183−190.
(48) Huang, W. L.; Zhu, Q. *Comput. Mater. Sci.* **2009**, *46*, 1076−1084.
(49) Huang, W. L. *Comput. Mater. Sci.* **2012**, *55*, 166−170.
(50) Nethercot, A. H., Jr. *Phys. Rev. Lett.* **1974**, *33*, 1088−1091.
(51) Tang, J.; Ye, J. *Chem. Phys. Lett.* **2005**, *410*, 104−107.
(52) Linsebigler, A. L.; Lu, G.; Yates, J. T. *Chem. Rev.* **1995**, *95*, 735−758.
(53) Paul, N.; Deka, A.; Mohanta, D. *J. Appl. Phys.* **2014**, *116*, 144902.